Int J Thermophys (2010) 31:2086–2102
DOI 10.1007/s10765-010-0888-4

Measurements of Speed of Sound in Lean and Rich Natural Gas Mixtures at Pressures up to 37 MPa Using a Specialized Rupture Tube

K. K. Botros

Received: 26 July 2010 / Accepted: 12 November 2010 / Published online: 1 December 2010
© Springer Science+Business Media, LLC 2010

Abstract Measurements of the speed of sound in 42 different compositions of lean, medium, and rich natural-gas mixtures using a specialized high-pressure rupture tube have been conducted. The rupture tube is made of stainless steel (internal diameter = 38.1 mm and length = 42 m), and is instrumented with 13 high-frequency-response dynamic pressure transducers (Endevco) mounted very close to the rupture end and along the length of the tube to capture the pressure-time traces of the decompression wave. Tests were conducted for initial pressures ranging from 10 MPa to 37 MPa and a temperature range from −25 °C to +68 °C. Gas mixture compositions were controlled by mixing conventional natural-gas mixtures from an adjacent gas pipeline with richer components of alkanes. Temperature control is achieved by a heat tracer along the tube with a set point at the desired gas temperature of the particular test. Uncertainty analysis indicated that the uncertainty in the experimentally determined speed of sound in the undisturbed gas mixture at the initial pressure and temperature is on the order of 0.306 %. The measured speeds of sound were compared to predictions by five equations of state, namely; the Benedict–Webb–Rubin–Starling (BWRS), AGA-8, Peng–Robinson (PR), Redlich–Kwong–Soave (RK–Soave), and Groupe Européen de Recherches Gaziéres (GERG-2004) equations.

Keywords Decompression wave speed · Dense phase · Dynamic pressure measurements · Equation of state · Fracture control · Natural gas mixtures · Rupture tube · Shock tube · Speed of sound · Thermophysical properties of gases

K. K. Botros (✉)
NOVA Research & Technology Center, 2928-16 Street N.E., Calgary, AB T2E 7K7, Canada
e-mail: botrosk@novachem.com

List of Symbols

C Speed of sound
D Pipe internal diameter
L Pipe length
$\#n$ Location number
P Gas pressure
P_i Initial gas pressure prior to rupture
s Entropy
t Time
T Temperature
T_i Initial gas temperature prior to rupture
X Axial distance
ρ Gas density

1 Introduction

Measurement of speed of sound can be carried out with relatively high accuracy, and it is therefore a useful parameter to check the reliability and performance of an equation of state. Analysis of the experimental and predicted data of speeds of sound in pure methane indicates that the uncertainty of the predicted speed of sound is higher at low temperatures and/or high pressures [1]. Unfortunately, high accuracy experimental data for natural gas mixtures are rather scarce. The most accurate and reliable data are those reported in [2–5]. In fact, AGA Report No. 10 [6] mentions only 17 natural gas mixtures for which measured speed-of-sound data were available. There is a need to extend the pool of experimental data on the speed of sound to allow further evaluation of the performance and predictability of the various equations of state.

One of the important parameters in pipeline fracture control is the decompression wave speed. Predictions of this parameter by gas decompression models, such as GASDECOM [7], are based on fundamental one-dimensional thermodynamic expansion behavior of the gas at the rupture point, independent of the pipe diameter [8,9]. The decompression wave speed can also be determined experimentally, either from a full scale rupture of a section of a pipeline, e.g., [10], or a simulated rupture using a small diameter rupture tube, e.g., [11–13]. In both methods, the decompression wave speed can be determined from pressure–time traces measured by high-frequency response transducers mounted at different locations along the pipe section. For any pressure level below the initial pressure, the time of arrival of the decompression wave at each successive pressure transducer can be determined, and the corresponding propagation speed can be calculated using a linear fit of distance from initiation against arrival time. Such calculations are repeated for progressively lower pressures. This is the format required for the application of the Battelle two-curve method for the determination of fracture arrest toughness [8,14,15]. In these decompression wave tests, a by-product of the experimental data is the speed of sound in the undisturbed gas mixtures in the tube, i.e., at the initial gas pressure and temperature. This can be determined by fitting the time of arrival of the frontal wave to each transducer location along the tube.

The present paper reports experimentally determined speed-of-sound values from a campaign of a total of 42 rupture tube tests on different mixtures of lean and rich natural gas at different pressures and temperatures. This rupture tube (42 m long, I.D. = 38.1 mm) is constructed at the TCPL Gas Dynamics Test Facility in Didsbury, Alberta, Canada. Results of the decompression wave speeds measured by this tube are reported in [11–13]. The experimentally determined speeds of sound for these 42 tests are reported here and are compared to five equations of state, namely, the Benedict–Webb–Rubin–Starling (BWRS) [16], AGA-8 [17], Peng–Robinson (PR) [18], Redlich–Kwong–Soave (RK–Soave) [19], and Groupe Européen de Recherches Gaziéres (GERG-2004) [20] equations.

2 Rupture Tube Setup

The rupture tube consists of four spool pieces of NPS 2 stainless-steel pipe making up a total length of 42 m, as shown in Fig. 1. They are made of NPS 2 × 11.1 mm WT, SCH XX, ASTM A312, 316 SS seamless tube (I.D. = 38.1 mm). All individual spools were designed for 41.370 MPa pressure, design factor = 0.8 and location factor = 0.625 (according to the latest edition of the CSA Standard Z662). ANSI 2500 RTJ flanges (PN 420 Standards) ASTM A182-316 SS were used. All spools were shop-tested to a minimum hydrostatic pressure of 62.055 MPa, and a maximum hydrostatic pressure of 62.755 MPa for a period of 1 h. Spool #4 is equipped with an automated blowdown and a pressure relief valve.

All spool pieces were internally honed to a roughness R_Z less than 25 microinches (0.635 μm). This surface roughness was achieved by a combination of grades and grit sizes of abrasive stones and use of a double spindle hone, and simultaneous rotation and reciprocation of the hone within the bore of the tube. Kerosene is used as a coolant and lubricant, and the final finish is achieved by a polishing/buffing head. Roughness measurements according to DIN 4768/1 were conducted using a Hommel Profile Stylus Model T500 at various locations inside the tube from both ends up to the maximum distance permitted by the Stylus reach.

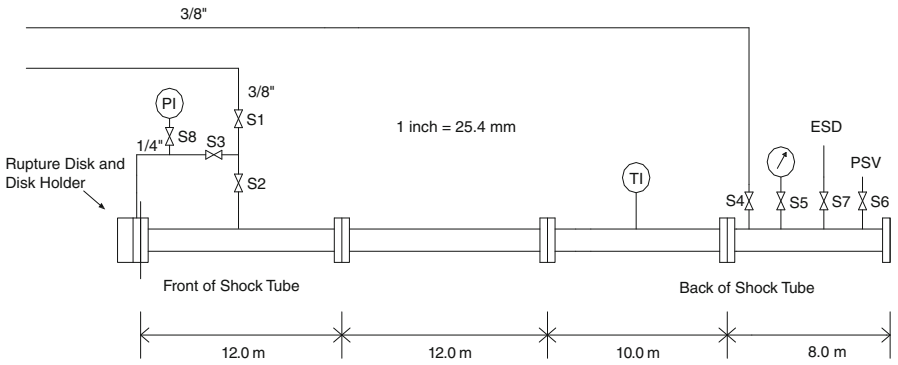

Fig. 1 Schematic of the rupture tube setup

Table 1 Location of the 13 Endevco pressure transducers mounted on spool #1 and temperature probes on spools #1, #2, and #3

Location	Distance (X) from choked location (mm)	Normalized distance (X/D)
1st Spool		
(Flange RF)	0	0.00
PT1	29.5	0.77
PT1A	92.4	2.43
PT1B	102.8	2.70
PT2	200	5.25
PT3	350	9.19
PT4	500	13.12
PT5	700	18.37
PT6	900	23.62
PT7	1 100	28.87
PT8	3 100	81.36
PT9	5 100	133.86
PT10	7 100	186.35
PT11	9 100	238.85
Temp (1)	4 000	104.99
2nd Spool		
Temp (2)	18 000	472.44
3rd Spool		
Temp (3)	23 000	603.67

A total of 16 Endevco dynamic pressure transducers are mounted along the length of the rupture tube, 13 of which are mounted on the front spool where the rupture disc is located. These transducers are mounted flush to the internal surface of the rupture tube to a tolerance of 0.0 mm to −0.2 mm using a specially designed fitting. Table 1 shows the locations of these pressure transducers measured from the raised face of the front flange, which is the location where the flow will choke following disc rupture. The exact locations of the pressure transducers on the front spool of the rupture tube were used in the determination of the speed of sound. There is also a static pressure transducer (by Yokogawa) mounted on spool #1. Two fast response temperature transducers (by Watlow) are located at indicated locations of spools #1 and #2, and a static temperature probe by Yokogawa on spool #3 (see locations in Table 1).

A rupture disc is placed at the front end of the tube, which, upon rupturing, causes a decompression wave to propagate up the 42 m pressurized rupture tube. The rupture discs used are commercial Fike SCRD BT FSR type, along with Fike's SRX rupture disc-holder. The discs are x-scored, which provides non-fragmenting rupture. The disc holder is made out of stainless steel and is designed to achieve a tight metal-to-metal seal, while maintaining tight rupture tolerances. Once the disc is ruptured, choked flow conditions will be established at the front surface of the front flange on the rupture tube. The open membrane area matches the I.D. of the disc holder which is 63.5 mm

in diameter, while the tube I.D. is 38.1 mm. This means that choking is guaranteed at the face of the aforementioned tube flange and not at the rupture disc. Additionally, the triangular pieces of the opened ruptured disc adhere to the rupture disc holder (I.D. = 63.5 mm).

Impulse and recoil motion of the rupture tube resulting from rupture of the disc could be both costly and dangerous if left unopposed. Therefore, tube motion is prevented by a concrete block backstop which weighs 16 tons, placed behind the far (flanged) end of the rupture tube. A rupture absorber consisting of alternate layers of steel/rubber plates is placed between the pipe and the backstop. Pipe recoil motion is prevented by four tensional chains fastened to the concrete backstop, and by additional straps at tube supports located every 1.5 m.

In order to control the temperature of the gas mixture in the rupture tube and to achieve a desired temperature before rupture, the rupture tube is heat traced and insulated with 50 mm thick insulation (thermal conductivity $= 0.036\ \mathrm{W \cdot m^{-1} \cdot K^{-1}}$). The heat tracer is rated for $300\ \mathrm{W \cdot m^{-2}}$, which translates to $56.8\ \mathrm{W \cdot m^{-1}}$ length of the rupture tube based on one run along the length of the tube.

The rupture tube is connected to an auxiliary system inside a heated building close to the tube. The auxiliary system includes a vacuum pump, a charge compressor which transfers base gas from the main facility high-pressure (5.5 MPa) gas loop into the rupture tube rig, as well as additional supplementary C2+ gas cylinders to make up the desired rich gas mixtures to be tested. The piping and instrumentation diagram for this auxiliary system is shown in Fig. 2. The design conforms to the requirements of the latest edition of CSA Standard Z662 for 41 MPa design pressure, 0.8 design factor, and 0.625 location factor. The vacuum pump is an Edwards Model # E2M30, which consists of a direct drive, rotary vane, double-stage vacuum pump, with a displacement of 22.3 cfm ($631\ \mathrm{L \cdot min^{-1}}$), pumping speed 19.5 cfm ($552\ \mathrm{L \cdot min^{-1}}$), and ultimate vacuum total pressure of 7.5×10^{-4} torr (without gas ballast). The charge

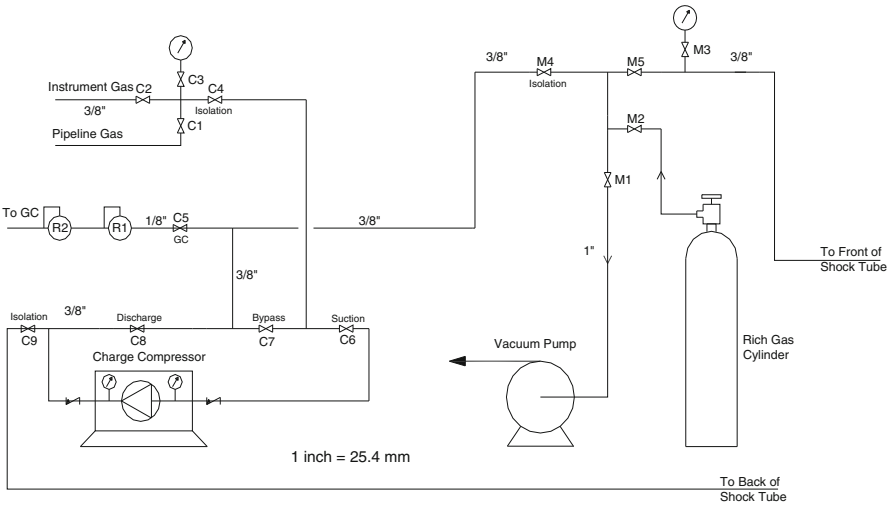

Fig. 2 Schematic of the rupture tube auxiliary system

compressor is a Haskel Gas booster model AGT-30/75 which consists of a large area reciprocating air driven piston directly coupled by a connecting rod to a small area gas piston. The compressor is capable of a discharge pressure up to 110 MPa (pressure ratio of 60:1).

A desired enriched gas mixture in the test section is attained by mixing gas from the adjacent pipeline loop (base gas) with a supplementary enriched gas from a pre-prepared mixture in a pressure cylinder. A simple mass balance calculation is performed to determine the amount and composition of the supplementary gas required, based on the main loop gas composition, the desired final composition, the volume of the test section together with the connecting system, and the final pressure. This calculation is also confirmed by actual measurement of the final gas composition by the on-line GC of a gas sample taken after recirculation.

3 Instrumentation and Test Procedure

The fast response pressure transducers are Endevco Model 8511A-5K piezoresistive pressure transducers, which are rated for safe operation up to 138 MPa, and for temperatures down to −73 °C. They are supplied with certificates of traceable calibration curves with an overall uncertainty of 40 kPa and a frequency response up to 20 kHz. They feature an active four-arm strain gage bridge diffused into a sculptured silicon diaphragm for maximum sensitivity and wideband frequency response. Endevco transducers also feature excellent linearity and high rupture resistance (138 MPa). Calibrations of these transducers are performed before and after rupture of each test using a Yokogawa pressure transmitter (Model EJA530A/HAC).

The temperature probes are Watlow fast response monolithic thermocouples together with Analog Devices AD594/AD595 amplifiers with cold junction compensation. The tip of the probe has been specially tapered from 1.65 mm down to 0.51 mm. The pressure isolation is provided by a standard 1/8 NPT (3.18 mm) "Swagelok" plug that has been drilled through, and the 1.65 mm probe has been welded into it. The response time is around 20 ms, and the uncertainty is 1 °C from −40 °C to +100 °C. They are calibrated against a static Yokogawa temperature transmitter (Model YTA110).

The data acquisition system is a HP E1431A and E1432A High Speed DAS, capable of ±0.7 % of reading in accuracy at 1 kHz, and the cross channel phase matching is ±0.125 deg. Data are collected in a block of 16 384 data points; hence, for a window of 320 ms, the data resolution is exactly 19.53 μs. The gas mixture composition is determined by an on-line Daniel 2350 gas chromatograph.

The test procedure involves eight main steps starting from evacuating the main decompression tube, associated header and tubing, up to the final step of rupturing the disc to atmosphere. These are: (1) purging with pipeline gas, (2) evacuation, (3) rich gas charge, (4) free flow to line pressure, (5) charge with the charge compressor up to 90 % of the burst pressure, (6) recycling the loop to ensure good mixing, (7) continuous gas sampling, and (8) disc rupture by means of increasing pressure in the tube. Temperature control is achieved by the heat tracer with a set point at the desired gas temperature of the particular test.

4 Scope of the Test Program

The test program consisted of a total of 42 tests conducted with various gas compositions representative of conventional natural gas mixture and other medium and rich mixtures, as shown in Table 2, along with the corresponding initial pressure and temperatures. Figure 3 shows phase envelopes for three selected gas mixtures representing the leanest, medium rich, and the richest gas mixtures among the 42 tested mixture compositions. These phase envelopes were calculated using the Peng–Robinson (PR) equation of state (EOS) as implemented in Aspen Plus V7.1 [21] The initial conditions (P_i and T_i) of the 42 gas mixtures are also shown in Fig. 3 to indicate the range of pressures and temperature of the test program.

5 Determination of the Speed of Sound

Figure 4 shows an example of the pressure–time traces as measured by the 13 pressure transducers along the first spool of the rupture tube. The experimentally determined speed of sound in the undisturbed mixture is obtained from the slope of the distance–time linear fit of the time of arrival of the decompression frontal wave at all locations of the pressure transducers identified inside the marked dotted bubble at the top of Fig. 4. Table 3 gives the exact time of arrival of the frontal wave at each transducer location, while Fig. 5 shows the resulting distance–time plot of these data. The slope of the linear fit to these data represents the speed of sound in the undisturbed gas mixture in the tube, which in this example of Test #16 was determined to be 629.117 $\mathrm{m \cdot s^{-1}}$.

As a matter of interest, but not essential for the present investigation, are the apparent kinks in the pressure–time profiles around 8 MPa in Fig. 4. This is a manifestation of the decompression wave isentrope crossing the phase envelope into the two-phase region. It is known that at a phase crossing, a sharp drop in the speed of sound occurs due to the dramatic drop in the thermodynamic derivative $(\partial P/\partial \rho)_s$.

6 Uncertainty Analysis

The uncertainty in the determination of the speed of sound from present measurements is introduced by the following four uncertainties:

(1) the uncertainty in the measurements of distances and time according to the following definition:

$$C = \frac{L_o}{t_o} \tag{1}$$

Hence,

$$\frac{\delta C}{C} = \sqrt{\left(\frac{\delta L}{L_o}\right)^2 + \left(\frac{\delta t_1}{t_o}\right)^2 + \left(\frac{\delta t_2}{t_o}\right)^2} \tag{2}$$

Table 2 Mixture compositions and conditions of the 42 rupture tube tests

Test #	Mixture composition (mol%)										P_i (kPa)	T_i (°C)
	C1	C2	C3	iC4	nC4	iC5	nC5	C6	N2	CO2		
1	98.6864	0.5822	0.0193	0.0000	0.0000	0.0000	0.0000	0.0000	0.5600	0.1521	18537.00	16.74
2	87.9168	6.5522	3.1044	0.2557	0.4785	0.0000	0.0000	0.0000	0.5062	1.1862	18584.00	21.50
3	85.8463	7.6575	3.8710	0.3638	0.7346	0.0000	0.0000	0.0000	0.4748	1.0520	10188.00	20.50
4	80.4083	7.3598	7.3078	0.8173	1.0930	0.0000	0.0000	0.0013	0.4619	2.5507	14182.00	12.20
5	82.2015	6.8193	7.4616	0.7052	0.8856	0.0000	0.0000	0.0014	0.4657	1.4598	19771.00	11.50
6	81.6402	7.2071	7.4769	0.7497	0.9701	0.0000	0.0000	0.0000	0.4668	1.4893	18175.00	11.90
7	82.9164	6.6487	7.0287	0.6657	0.8908	0.0000	0.0000	0.0000	0.4733	1.3765	21171.00	−3.51
8	79.3017	10.0013	6.1103	1.3280	1.7365	0.0000	0.0000	0.0000	0.4500	1.0723	21344.00	−14.01
9	97.2754	1.4365	0.2669	0.0321	0.0432	0.0101	0.0075	0.0092	0.5555	0.3635	18438.00	17
10	87.8025	6.6332	3.1394	0.2659	0.5590	0.0083	0.0054	0.0116	0.5302	1.0443	18107.00	20.30
11	84.9846	8.4616	3.9098	0.3707	0.8793	0.0100	0.0073	0.0084	0.4879	0.8803	9841.00	21.10
12	79.9364	7.6781	7.2167	0.8956	1.2097	0.0063	0.0045	0.0062	0.4636	2.5830	14419.00	10.95
13	82.3030	6.8675	7.1335	0.7524	0.9859	0.0067	0.0047	0.0064	0.4743	1.4656	19837.00	11.37
14	81.8606	7.0709	7.1443	0.8004	1.0397	0.0076	0.0056	0.0071	0.4696	1.5941	19708.00	11.15
15	83.7591	6.3948	6.4735	0.6678	0.9945	0.0077	0.0055	0.0073	0.4800	1.2097	21237.00	−4.50
16	78.7514	10.4724	5.9904	1.3927	1.8635	0.0060	0.0043	0.0060	0.4448	1.0687	21451.00	−10.19
17	91.1099	5.3291	1.4813	0.1562	0.2119	0.0496	0.0378	0.0413	0.5768	1.0060	36195.20	26.50
18	86.7053	5.2082	3.5972	0.9534	0.2175	0.9484	0.5758	0.2788	0.5506	0.9648	36296.00	28.70
19	88.5093	4.1255	1.0465	0.1181	0.1658	0.0361	0.0280	0.0320	0.5761	5.3626	35511.06	20.70
20	92.4035	4.4323	1.2201	0.1387	0.1916	0.0414	0.0311	0.0370	0.6169	0.8874	36181.72	18.00

Table 2 continued

Test #	Mixture composition (mol%)										P_i (kPa)	T_i (°C)
	C1	C2	C3	iC4	nC4	iC5	nC5	C6	N2	CO2		
21	83.1579	4.3151	5.7600	0.9862	1.9957	1.4712	0.6350	0.3017	0.5687	0.8084	36333.65	20.50
22	83.1355	4.9189	5.5617	0.9764	1.8895	1.4019	0.5925	0.2741	0.4847	0.7647	36114.00	67.90
23	76.4542	9.3231	6.0851	1.4975	3.3347	0.8439	0.8289	0.4420	0.5150	0.6756	33377.00	21.20
24	80.6894	7.7610	5.5969	0.9729	1.8834	1.0027	0.5101	0.3469	0.5171	0.7196	35658.00	21.20
25	92.1755	4.6099	1.2039	0.1378	0.1810	0.0410	0.0314	0.0398	0.6761	0.9036	18072.00	5.89
26	88.6070	6.2242	2.5440	0.3941	0.6132	0.0383	0.0297	0.0336	0.6211	0.8948	20635.00	9.71
27	88.5176	6.0391	2.6463	0.4618	0.7343	0.0400	0.0306	0.0490	0.5926	0.8887	17857.00	22.08
28	88.1669	6.4552	2.7242	0.4346	0.6854	0.0362	0.0273	0.0343	0.6029	0.8330	16675.00	12.57
29	88.2524	6.4420	2.6008	0.4253	0.6545	0.0381	0.0293	0.0343	0.6088	0.9145	9669.00	4.84
30	86.6688	5.5999	4.4932	0.4516	1.2275	0.0326	0.0237	0.0205	0.5760	0.9062	17924.00	19.04
31	71.2440	17.6126	9.6512	0.1026	0.1327	0.0320	0.0243	0.0340	0.4533	0.7133	18598.00	12.21
32	0.0000	0.0000	0.0000	0.0000	0.0000	0.0000	0.0000	0.0000	100.0000	0.0000	10059.04	−12.71
33	95.4741	2.9363	0.1902	0.0156	0.0253	0.0041	0.0030	0.0013	0.5689	0.7812	10580.78	−25.59
34	94.9862	3.4233	0.2054	0.0163	0.0263	0.0041	0.0031	0.0015	0.5646	0.7692	14667.25	−15.74
35	95.1265	3.2879	0.2041	0.0165	0.0265	0.0043	0.0033	0.0013	0.5656	0.7640	20545.00	−24.80
36	79.3089	14.1967	5.2556	0.0114	0.0164	0.0029	0.0020	0.0009	0.5513	0.6539	9940.19	0.06
37	76.4932	16.6273	5.7453	0.0121	0.0172	0.0030	0.0021	0.0012	0.4571	0.6415	14210.82	4.61
38	80.7368	13.1536	4.9021	0.0186	0.0187	0.0034	0.0025	0.0012	0.4707	0.6924	19510.96	−12.37
39	68.5085	21.4056	9.0804	0.0258	0.0142	0.0024	0.0018	0.0007	0.4079	0.5527	9949.48	−4.99
40	68.0095	20.7126	10.3324	0.0132	0.0200	0.0035	0.0027	0.0015	0.6889	0.2157	14113.86	3.01
41	69.2837	19.2272	10.4189	0.0302	0.0159	0.0028	0.0022	0.0010	0.4052	0.6129	19597.13	−3.89
42	70.7121	19.6437	7.9905	0.1234	0.1237	0.0252	0.0182	0.0158	0.5736	0.7738	7580.00	3.00

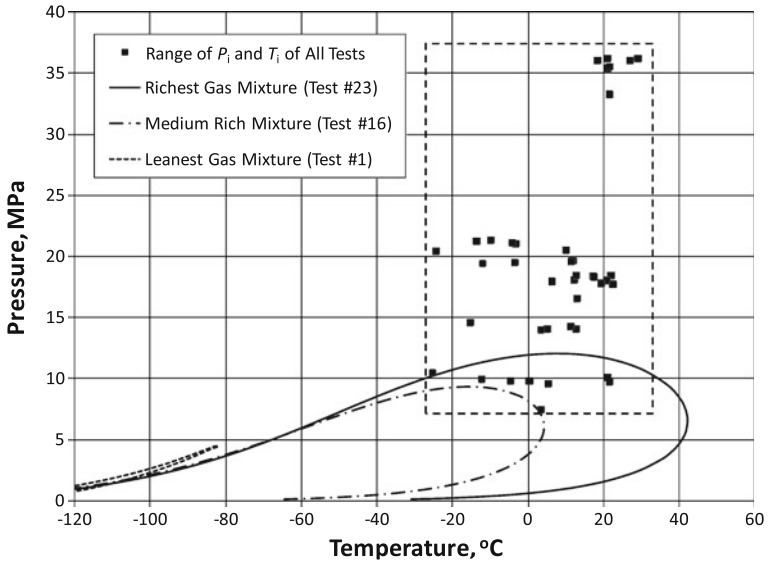

Fig. 3 Ranges of pressure and temperature of the test program and phase envelopes of selected lean, medium and rich gas mixtures based on PR E.O.S

where L_o is the distance used in the determination of the speed of sound and t_o is the time between signals from the transducers a distance (L_o) apart.
The uncertainty δt has two components, namely,

δt_1 is the uncertainty due to resolution of the data acquisition system, and hence, the uncertainty in the determination of the time of arrival of the frontal wave and

δt_2 is the uncertainty due to *filtering*/smoothing of the pressure–time profile.

(2) the uncertainty in the pressure
(3) the uncertainty in the temperature
(4) the uncertainty in the mixture composition, which is assumed to be 2 % of the mol% value of all components in the mixture except for C1, which has the lowest uncertainty of 0.2 %.

Table 4 gives estimated values for the above individual uncertainties based on the linear fit of the 13 X–t points of Fig. 5. It is shown that the uncertainty in the speed of sound is estimated at 0.306 %, and the main contributor to it is δt_1 (uncertainty due to resolution of the data acquisition system), and the uncertainty in mixture composition.

7 Results

The speed of sound resulting from all of the 42 tests conducted on the rupture tube is given in Table 5. Predictions of the speed of sound by different equations of state are also reported for each test and the corresponding deviation (error) from the measured values. Here the deviation in the EOS prediction is defined as

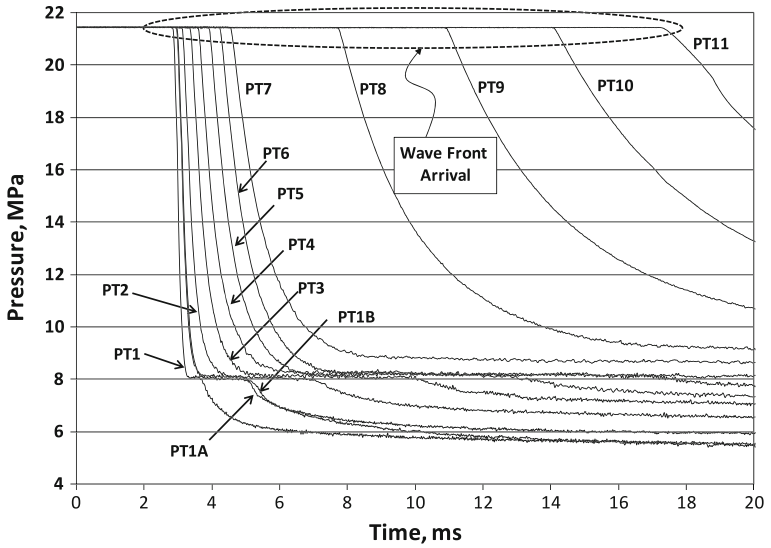

Fig. 4 Example of pressure–time traces for Test #16

Table 3 Example of arrival time of the wave front at the 13 transducer locations in Test #16

Location	Time (ms)	X (mm)
PT1	2.8125	28.8
PT1A	2.929688	97.5
PT1B	2.96875	106.5
PT2	3.105469	202
PT3	3.359375	350.5
PT4	3.574219	500.4
PT5	3.886719	700.4
PT6	4.179688	899.9
PT7	4.53125	1100.3
PT8	7.695312	3100
PT9	10.859375	5100
PT10	14.082031	7100
PT11	17.246094	9100

$$\text{Deviation (\%)} = \left(\frac{C_{\text{EOS}} - C_{\text{m}}}{C_{\text{m}}}\right) \times 100 \tag{3}$$

where C_{EOS} is the value of the speed of sound predicted by the EOS and C_{m} is the value of the speed of sound determined from measurements by the present rupture tube.

The first equation of state is the BWRS which is based on a virial EOS [16] that was developed for light gases and hydrocarbons. It is an 11-parameter, non-cubic equation of state. Mixing rules are defined in terms of a single binary interaction parameter for

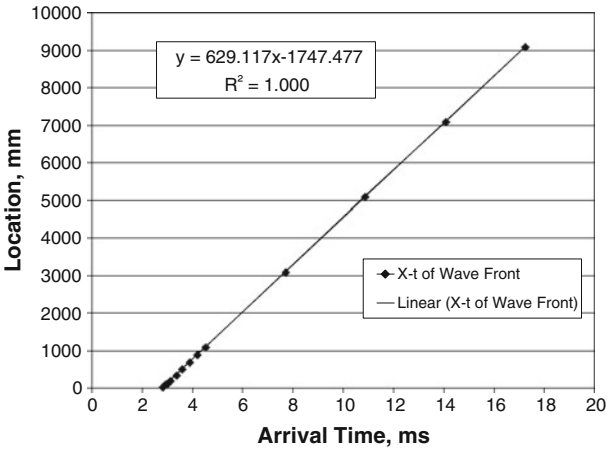

Fig. 5 Linear fit of the arrival time–axial distance for Test #16 (slope = speed of sound)

Table 4 Uncertainty analysis in determining the speed of sound from the rupture tube tests

Parameter	Value	Units
P_i (Test #23)	33 377	kPa
T_i (Test #23)	21.2	°C
t_o	18	ms
L_o	9 100	mm
dL	2	mm
dt_1 (resolution in Data Acquisition)	39.06	μs
dt_2 (due to filtering/smoothing)	9.77	μs
dL/L_o	0.0220	%
dt_1/t_o	0.2170	%
dt_2/t_o	0.0543	%
(1) Uncertainty in speed of sound due to geometry and time	0.225	%
(2) Uncertainty in speed of sound due to 0.1% uncertainty in pressure	0.050	%
(3) Uncertainty in speed of sound due to 0.5 °C uncertainty in temperature	0.085	%
(4) Uncertainty in speed of sound due to mixture composition	0.183	%
Total uncertainty (1 through 4 above)	0.306	%

each binary mixture. The pure-component parameters and binary interaction parameters used in this EOS are those of Hopke and Lin [22]. The values of the speed of sound by this EOS were obtained from the version implemented in GASDECOM [7]. The second equation of state is AGA-8 [17] which is also based on a virial, 11-parameter, non-cubic equation of state, with pure fluid ideal heat capacities, enthalpies and entropies based on Aly and Lee equations [23]. Mixing rules are defined in terms of a single binary interaction parameter for each binary mixture. The pure-component parameters and binary interaction parameters used in this EOS are defined in [6,17]. The third EOS is Peng–Robinson (PR) [18], which is a cubic equation of state, and is widely

Table 5 Comparison between the measured speed of sound by the rupture tube and predicted values by different equations of state

Test #	Speed of sound ($m \cdot s^{-1}$)	Deviation (%)				
	Rupture tube	BWRS	AGA-8	PR	RK–Soave	GERG
1	502.89	0.56	0.50	2.37	2.48	0.45
2	479.38	0.57	0.59	2.59	2.99	0.75
3	377.74	1.45	1.74	4.42	5.82	1.51
4	403.12	1.21	1.52	5.29	6.53	0.89
5	513.31	−0.26	0.53	0.73	1.07	1.19
6	483.92	−0.34	0.40	1.65	2.26	0.84
7	579.80	−0.57	0.69	−1.70	−2.05	1.44
8	644.80	−0.42	0.72	−4.32	−5.23	1.07
9	498.70	0.36	0.31	2.25	2.40	0.30
10	474.42	0.31	0.31	2.49	2.95	0.45
11	379.96	−0.20	0.09	2.61	4.02	−0.13
12	408.29	1.03	1.50	5.16	6.41	0.98
13	514.28	−0.21	0.57	0.74	1.07	1.13
14	513.52	−0.45	0.40	0.59	0.94	1.12
15	582.21	−0.52	0.67	−1.72	−2.11	1.46
16	629.12	0.39	1.21	−3.40	−4.14	1.73
17	716.33	0.53	1.00	−2.62	−4.13	1.34
18	717.03	0.75	1.10	−3.14	−4.34	2.17
19	699.99	0.33	1.06	−2.94	−4.30	1.22
20	727.94	1.08	1.68	−2.36	−4.10	1.91
21	755.13	0.45	0.68	−4.90	−6.19	1.37
22	661.38	−0.65	−0.84	−3.35	−3.70	0.72
23	736.54	0.69	0.51	−5.52	−6.45	0.95
24	754.57	−0.17	−0.03	−5.62	−6.82	0.48
25	488.73	0.96	0.39	2.28	2.47	0.61
26	523.87	1.04	0.70	1.21	1.20	1.37
27	470.74	1.12	0.17	2.49	2.99	0.31
28	456.88	1.35	0.54	3.20	3.77	0.59
29	371.18	1.37	1.17	4.27	5.66	0.91
30	479.83	−1.03	−1.79	0.33	0.88	−1.59
31	513.90	1.07	0.67	0.19	0.75	1.30
32	353.49	0.17	−0.25	0.36	1.26	−0.02
33	387.09	1.39	0.18	4.86	5.83	−0.52
34	449.13	1.55	1.24	4.26	4.58	1.00
35	592.19	0.27	0.91	−1.31	−2.40	1.62
36	350.17	1.67	1.04	5.82	7.35	−0.01
37	420.36	2.03	1.39	4.97	6.14	0.77

Table 5 continued

Test #	Speed of sound ($m \cdot s^{-1}$)	Deviation (%)				
	Rupture tube	BWRS	AGA-8	PR	RK–Soave	GERG
38	582.54	0.25	0.46	−2.14	−2.62	1.14
39	348.38	2.41	1.82	8.71	11.21	−1.94
40	444.07	2.18	1.83	3.92	5.21	1.33
41	614.59	0.12	−0.34	−4.87	−5.28	−0.27
42	309.87	1.33	1.32	5.06	6.92	0.56

used because of its relatively simple mathematical structure with only two coefficients defined in terms of the critical pressure, critical temperature, and the acentric factor of the pure substance. Mixing rules are defined in terms of a single binary interaction parameter for each binary mixture. The values of the speed of sound by this EOS were obtained from the version implemented in REFPROP developed by NIST [24]. The fourth EOS is Redlich–Kwong–Soave (RK–Soave) [19], which is also a cubic equation of state. The values of the speed of sound by this EOS were obtained from the version implemented in Aspen Plus v7.1 [21]. The fifth EOS is Groupe Européen de Recherches Gaziéres (GERG-2004) [20], which was developed by Ruhr-Universität Bochum. The normal range of validity of GERG-2004 is temperatures from 90 K to 450 K and pressures up to 35 MPa, although it is further restricted for some components. The GERG-2004 EOS is based on pure-substance equations of state for each of the considered mixture components and correlation equations for binary mixtures consisting of these components; both are expressed in terms of the Helmholtz free energy as a function of temperature and density. The values of the speed of sound by this EOS were obtained from the version implemented in REFPROP [24].

Figure 6 shows the deviations in the predictions of the speed of sound by the above five EOS for all of the 42 rupture tube test conditions and mixture compositions. It is shown that the deviations in predictions of the speed of sound by BWRS, AGA-8, and GERG-2004 EOS are within ±2 %. The mean deviation for these three EOS lies between 0.6 % and 0.77 %, and the standard deviation between 0.71 % and 0.83 % are shown in Table 6. However, the mean of the absolute deviation of these three EOS is between 0.83 % and 0.99 %, with the standard deviation between 0.52 % and 0.59 %.

This performance is not matched by the PR or RK–Soave cubical EOS. For these two EOS, it is shown that the deviations in predictions of the speed of sound can exceed 5 % to 6 %. Although the mean deviation for these two EOS is between 0.78 % and 0.98 %, the standard deviation is quite high (between 3.6 % and 4.6 %) as shown in Table 6. Likewise, the mean of the absolute deviation of these two EOS is also high, between 3.1 % and 4.0 %, with the standard deviation between 1.8 % and 2.3 %.

It should be pointed out that Tests #17 through #24 involve much higher pressures (33 377 kPa to 36 333 kPa) than the rest of the tests. The deviations in the speed of sound for these tests by both PR and RK–Soave EOS are consistent and are in the range of −4 % to −7 %, while the other three EOS are within the deviation limits of ±2 %.

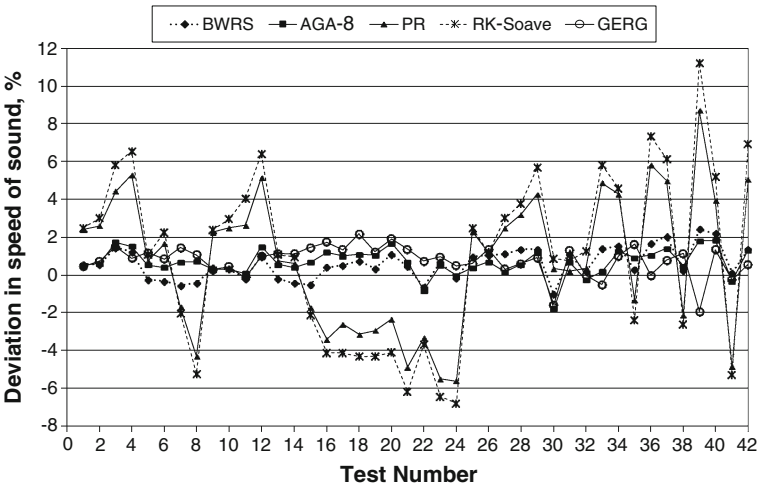

Fig. 6 Deviations in speed-of-sound predictions by different equations of state (reference is measurements by the rupture tube)

Table 6 Deviations of the various equations of state in predicting the speed of sound based on the 42 rupture test conditions

	Deviation (%)		Absolute deviation (%)	
	Mean	St. Dev.	Mean	St. Dev.
BWRS	0.600	0.825	0.828	0.589
AGA-8	0.676	0.713	0.830	0.520
PR	0.784	3.616	3.160	1.863
RK–Soave	0.983	4.550	4.024	2.260
GERG	0.774	0.821	0.988	0.537

Finally, Test #32 is a reference test conducted on pure nitrogen. The deviations in the speed of sound as predicted by four out of the five EOS, namely BWRS (0.173 %), AGA-8 (−0.245 %), PR (0.359 %), and GERG-2004 (−0.017 %) are quite low and are within the uncertainty in the measurements. However, the prediction by the RK–Soave EOS still shows a relatively high deviation (1.255 %).

8 Concluding Remarks

The following conclusions can be drawn from the present measurements and prediction results:

1. Measurements of the speed of sound in natural gas mixtures can be achieved with a rupture tube test to an uncertainty within 0.306 %.
2. Predictions of the speed of sound by BWRS, AGA-8, and GERG equations are consistent and within ±2 % of those measured by the present rupture tube. The

deviations in predictions of the speed of sound by these three EOS are between 0.6 % and 0.77 %, and the standard deviation between 0.71 % and 0.83 %.

3. The performance of the other two cubical EOS (PR and RK–Soave) is relatively rather poor and show deviations in predictions of the speed of sound exceeding 5 % to 6 %. Although the mean deviation for these two EOS is between 0.78 % and 0.98 %, the standard deviation is quite high (between 3.6 % and 4.6 %).
4. The above findings have significant implications when these EOS are used in the prediction of the decompression wave speed required for fracture control and design of natural-gas pipelines. They also reflect on the performance and reliability of these EOS in so far as derived intrinsic thermodynamic properties of natural gas mixtures.

Acknowledgments The author wishes to thank the sponsors of this program: Sonangol's AnLNG Pipeline Project, TransCanada Pipelines (TCPL), the Australian Pipeline Industry Association Research and Standards Committee (APIA RSC), Alliance Pipeline Ltd., PRCI, and the Japanese Gas Association. Special thanks are due to Gerard Lalonde (TCPL) for his creativity in the unique design of the rupture tube, to John Geerligs (NRTC) for performing the rupture tests, and to Doug Mantai for overseeing the safety protocols at TCPL Gas Dynamics Test Facility in Didsbury, Alberta, Canada. Assistance offered by several staff members of NRTC during testing is acknowledged. Aspen Plus simulations to determine the speed of sound based on the RK-Soave EOS by Claire Ennis (NRTC) is gratefully acknowledged. Invaluable discussion with B. Rothwell, R.J. Eiber, L. Carlson, L. Fletcher, and T. Robinson during the course of this test campaign is much appreciated.

References

1. W. Studzinski, M.H. Weiss, K.K. Botros, in *Critical Flow Factor For Natural Gas*. 2nd International Conference on Flow Measurement, London, UK (1988)
2. B.A. Younglove, N.V. Fredrick, R.D. McCarty, NIST Monograph 178 (1993)
3. B.E. Gammon, D.R. Douslin, J. Chem. Phys. **64**, 203 (1976)
4. A. Sivaraman, B.E. Gammon, Speed of Sound Measurements in Methane, NIPER-142 (1986)
5. G.C. Straty, Cryogenics **15**, 729 (1975)
6. Transmission Measurements Committee, Speed of Sound in Natural Gas and Other Related Hydrocarbon Gases, American Gas Association Report No. 10 (2003)
7. R. Eiber, T. Bubenik, W.A. Maxey, in *Fracture Control Technology for Natural Gas Pipelines*. GASDECOM, computer code for the calculation of gas decompression speed, NG-18 Report 208, AGA Catalogue No. L51691 (1993)
8. R.J. Eiber, T.A. Bubenik, W.A. Maxey, Fracture Control for Natural Gas Pipelines, PRCI Report, Catalogue No. L51691 (1993)
9. R.J. Eiber, L. Carlson, B. Leis, Fracture Control Requirements for Gas Transmission Pipelines, in *Proceedings 4th International Conference on Pipeline Technology Ostend* (Scientific Surveys, Beaconsfield, UK, 2004), p. 437
10. R.J. Eiber, W.A. Maxey, *Full-Scale Experimental Investigation of Ductile Fracture Behaviour in Simulated Arctic Pipeline*, Materials Engineering in the Arctic (ASM, Metals Park, OH, 1977), p. 306
11. K.K. Botros, J. Geerligs, R.J. Eiber, ASME J. Press. Vessel Technol. **132**, 051303 (2010)
12. K.K. Botros, W. Studzinski, J. Geerligs, A. Glover, Can. J. Chem. Eng. **82**, 880 (2004)
13. K.K. Botros, J. Geerligs, J. Zhou, A. Glover, Int. J. Press. Vessels Pip. **84**, 358 (2007)
14. W.A. Maxey, J.C. Kiefner, R.J. Eiber, A.R. Duffy, in *Ductile Fracture Initiation, Propagation and Arrest in Cylindrical Vessels*, Fracture Toughness ASTM STP 514 (ASTM, West Conshohocken, PA, 1972), p. 70
15. W.A. Maxey, in *Fracture Initiation, Propagation and Arrest*, 5th Symposium on Line Pipe Research, PRCI Catalogue No. L30174 (1974), p. J-1
16. K.E. Starling, *Fluid Thermodynamic Properties for Light Petroleum Systems* (Gulf Pub., Houston, TX, 1973)

17. J. Savidge, S. Beyerlein, E. Lemmon, K. Starling, Natural Gas Density and Compressibility Factor—Executable Program and Fortran Code, American Gas Association Report No. 8, Version 1.2 (1994)
18. D.Y. Peng, D.B. Robinson, Ind. Eng. Chem. Fundam. **15**, 59 (1976)
19. G. Soave, Chem. Eng. Sci. **27**, 1197 (1979)
20. O. Kunz, R. Klimeck, W. Wagner, M. Jaeschke, The GERG-2004 Wide-Range Equation of State for Natural Gases and Other Mixtures, Groupe Européen de Recherches Gaziéres (GERG), GERG TM15 (2007)
21. AspenTech, *Aspen Plus® V7.1 Simulation Engine*, 200 Wheeler Road, Burlington, MA 01803. http://www.aspentech.com/
22. S.W. Hopke, C.J. Lin, in *Application of BWRS Equation to Natural Gas Systems*, 76th National AIChE Meeting, American Institute of Chemical Engineers, Tulsa, OK (1974)
23. F.A. Aly, L.L. Lee, Fluid Phase Equilib. **6**, 169 (1981)
24. NIST Standard Reference Database 23, *NIST Reference Fluid Thermodynamic and Transport Properties Database* (*REFPROP*): *Version 8.0* (National Institute of Standards and Technology, Boulder, CO, 2007), www.nist.gov/ts/msd/srd/nist23.cfm